From test data to FE code: a straightforward strategy for modelling the structural bonding interface

M. A. Lepore, M. Perrella
Department of Industrial Engineering, University of Salerno, via Giovanni Paolo II, 132 - 84084 - Fisciano (SA), Italy
malepore@unisa.it, mperrella@unisa.it

ABSTRACT. A straightforward methodology for modelling the cohesive zone (CZM) of an adhesively bonded joint is developed, by using a commercial finite element code and experimental outcomes from standard fracture tests, without defining a damage law explicitly. The in-house developed algorithm implements a linear interpolated cohesive relationship, obtained from literature data, and calculates the damage at each step increment. The algorithm is applicable both to dominant mode I or dominant mode II debonding simulations. The hypothesis of unloading stages occurrence is also considered employing an irreversible behaviour with elastic damaged reloading. A case study for validation is presented, implementing the algorithm in the commercial finite element method (FEM) software Abaqus®. Numerical simulation of dominant mode I fracture loading provides with satisfactory results.

KEYWORDS. Finite element method; Mode I crack; Fracture toughness; Cohesive law; Adhesive bonding.

Citation: Lepore, M. A., Perrella, M., From test data to FE code: a straightforward strategy for modelling the structural bonding interface, Frattura ed Integrità Strutturale, 39 (2017) 191-201.

Received: 10.06.2016
Accepted: 10.10.2016
Published: 01.01.2017

INTRODUCTION

Nowadays, structural bonding is widely used as joining technique in many engineering fields. Safety requirements are often to be satisfied, as for example in civil applications where FRP laminates are anchored to beams for strengthening purposes and seismic retrofitting [1]; in superconducting systems where insulating composite wraps are bonded to superconducting cables subjected to Lorentz forces [2]; in aeronautical and automotive structures for repairing process [3]. There are numerous advantages with respect to traditional mechanical fastening methods: homogeneous distribution of stresses throughout the union, reduction of the joint weight, sealing function and protection against corrosion, excellent fatigue strength, free design of the joint, and so on. However, the application of this technique to high-technology industry requires the satisfaction of a large number of requirements especially about the adhesive joining durability and reliability. Thus, a proper description of mechanical behaviour, and the prediction of fracture propagation at the interface is necessary in order to realize a correct design phase of adhesively bonded structures. Continuum damage mechanics (CDM) offers suitable tools for facing this issue, in coupling with the FE methodology. Using such approach the proper definition of a representative volume element (RVE) is crucial because its dimension relates the relevant scales in which the fracture process and the softening behaviour take place. A careful choice of the

RVE dimension makes this approach versatile enough to deal with a plenty of practical problems, among which, as examples, we can cite the homogenization of an RVE as a step for multiscale modelling [4]; the damage and failure modelling of inhomogeneous micro-structured materials under quasi static load [5]; the damage evolution and failure modelling of homogeneous materials under creep conditions [6]. The cohesive zone modelling (CZM) approach can be considered as a special case of the CDM methodology in which the softening behaviour is confined to an interface domain and the RVE dimension is implicitly taken into account by the material law. Among the methodologies for studying decohesion processes, the CZM approach is relevant in many engineering applications, from the simple debonding of a cantilever beam [7], to the three-dimensional delamination modelling in a cracked FML full scale aeronautic panel [8]. This method is based on the definition of a cohesive zone law, i.e. the traction-separation relationship at the bonded surface of the joint. For basic modes of debonding, the CZM can be estimated with experimental data from suitable test campaigns. Once defined, both in a direct or indirect way, it can be implemented in a Finite Element code for simulating the debonding phase.

Many cohesive traction-separation laws are reported in literature by using experimental, theoretical, and computational techniques. Among them, a large number concerns the response in normal (mode I) and shearing (mode II and III) direction with respect to the interface and under mixed mode I-II loading condition, whilst pure mode III or mixed mode II-III are less investigated. In order to evaluate experimentally the constitutive, peel, properties of adhesive and adherends, both metallic and composite, several standard test methods use the double cantilever beam (DCB) specimen under mode I fracture loading. Olsson et al. [9] developed an analytical solution for the determination of the constitutive properties of thin interphase layers, which provides with reliable results for non rigid adherends. Sorensen et al. [10] presented a traction-separation relation, based on the J-integral approach, for DCB. Valoroso et al. [11] proposed a deterministic identification of mode I cohesive parameters for bonded interfaces that overcomes the difficulties and limitations of ISO 25217 standard test. Stigh et al. [12] proposed an alternative experimental method to determine the complete cohesive relation of a thin adhesive layer loaded in peel with the same DCB specimen. Shen et al. [13], instead, implemented digital image correlation (DIC) technique to measure displacements at the crack tip in order to evaluate fracture parameters and determine cohesive relationships. Fernandes et al. [14] analysed mode II cohesive relationship of carbon–epoxy composite bonded joints using DIC and the direct method applied to the end notched flexure (ENF) test. Mode II and mixed mode I-II testing were also analysed in [15, 16]. A mode III traditional test methodology was presented in [17]. Cricrì et al. [18] presented a methodology, based on an innovative test device, for studying bonded elements subjected to pure mode III loading condition.

The present work describes a straightforward strategy for modelling the structural bonding interface of a joint using a commercial FEM code, assuming that the loading modes are uncoupled. Such an approach is implemented in an algorithm and a validation study case is presented by using the software Abaqus.

THEORETICAL BACKGROUND

In a 2D problem, the traction vector $\boldsymbol{T}$, whose components σ and τ, respectively acting on the interface along normal n and tangential s direction, can be expressed in matrix form as:

$$\boldsymbol{T}=\begin{bmatrix}\sigma\\ \tau\end{bmatrix}=\boldsymbol{K}\cdot\boldsymbol{u}=\begin{bmatrix}K_{nn} & K_{ns}\\ K_{sn} & K_{ss}\end{bmatrix}\begin{bmatrix}\delta_n\\ \delta_s\end{bmatrix} \tag{1}$$

where K_{nn}, and K_{ss} are stiffness terms, while δ_n and δ_s are normal and tangential separations, respectively. In particular, separations are numerically equal to the jump displacements of the cohesive elements. The initial (undamaged state) stiffness components of K_{nn} and K_{ss} are respectively equal to the ratio between Young's modulus and adhesive thickness and the ratio between shear modulus and adhesive thickness whereas $K_{sn} = K_{ns} = 0$. In general, during the phase of interface opening, the stiffness parameters vary, decreasing their values with damage increasing. Therefore, the damage law defines the stiffness terms. When σ and τ are considered uncoupled, the mixed elastic terms in Eq. (1), K_{ns} and K_{sn}, are set to null values.

Many effective traction-separation laws valid for pure loading modes or uncoupled cohesive behaviours are available in literature. Among these, one of the simplest, sometimes also available in commercial FEM codes, is the bilinear (linear softening) relationship. Three points of the traction-separation curve define this model (origin, maximum and final points) whilst the area under the curve represents the critical fracture energy G_c (Fig. 1). In the first section of the curve, two

hypothesis are assumed: there is no damage at the material interface (adhesive) and displacements and strains are elastic. In the second section, instead, the adhesive undergoes progressive damage up to the reaching of a limit value, corresponding to the occurrence of the maximum allowable deformation. In this section, the stress, normal respect to the displacement direction, decreases. Beyond this limit value, the stress has null values.

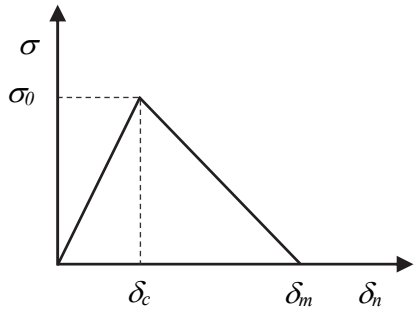

Figure 1: Bilinear traction-separation relationship for mode I loading condition.

The vertex, corresponding to the ending point of linear elastic section, represents the starting point of damage process. The damage function, which relates the separation within the cohesive elements to the corresponding tractions, is initially set to zero and reaches its maximum value, equal to one, in correspondence of the maximum displacement at the interface, i.e. the point of maximum damage. The cohesive law for mode I (or mode II) fracture process is defined by only three parameters:

1) the initial stiffness K_0, which physically is the slope of the elastic section;
2) the traction σ_0 at the interface or the separation δ_c within the cohesive elements, in correspondence of which the damage process starts;
3) the critical energy release rate G_c or the displacement at the failure δ_m.

The mathematical formulation of bilinear cohesive law is the following:

$$\sigma = \begin{cases} K_0\delta_n,\ 0 \le \delta_n \le \delta_c \\ \dfrac{\sigma_0}{(\delta_c - \delta_m)}(\delta_n - \delta_m),\ \delta_c \le \delta_n \le \delta_m \\ 0,\ \delta_n > \delta_m \end{cases} \qquad (2)$$

$$G_c = \frac{1}{2}\sigma_0\delta_m$$

Tvergaard et al. [19] proposed a tri-linear relationship, more accurate for ductile adhesives. As previously, the first section grows linearly reaching the damage initiation process in correspondence of a critical separation δ_{c1}. The traction remains constantly equal to its maximum value in the range [δ_{c1}, δ_{c2}] and then decreases after the critical separation δ_{c2}. The shape of trapezoidal function is shown in Fig. 2, while it is mathematically expressed as follows:

$$\sigma = \begin{cases} \dfrac{\sigma_0}{\delta_{c1}}\delta_n,\ 0 \le \delta_n \le \delta_{c1} \\ \sigma_0,\ \delta_{c1} \le \delta_n \le \delta_{c2} \\ \dfrac{\sigma_0}{(\delta_{c2} - \delta_m)}(\delta_n - \delta_m),\ \delta_{c2} \le \delta_n \le \delta_m \\ 0,\ \delta_n > \delta_m \end{cases} \qquad (3)$$

$$G_c = \frac{1}{2}\sigma_0\left(\delta_m + \delta_{c2} - \delta_{c1}\right)$$

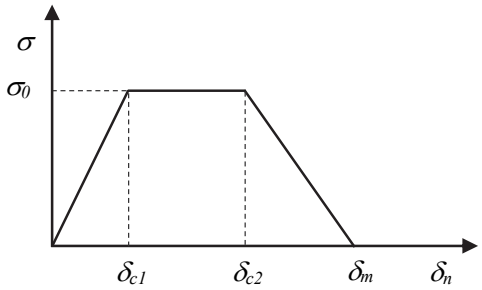

Figure 2: Trilinear traction-separation relationship for mode I loading condition.

Another often used traction-separation model is the exponential relationship (Fig. 3), proposed by Needleman et al. [20].

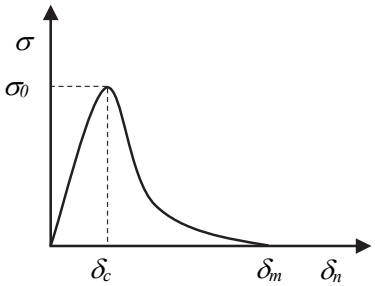

Figure 3: Exponential traction-separation relationship for mode I loading condition.

This model consists of a continuous and smooth exponentially decaying function, having the following formulation:

$$\sigma = G_c \frac{\delta_n}{\delta_c^2} e^{-\frac{\delta}{\delta_c}} \tag{4}$$

In the exponential model, the damage process begins with the displacement $\delta_n = 0$, whereas in the previously described laws the damage initiation starts after the reaching of a critical separation value or of the corresponding maximum stress occurrence.

For all the above models, a damage variable D is also defined, depending on the maximum separation currently achieved, δ_{max}. Such variable can be conveniently expressed in terms of current versus initial stiffness, as:

$$D = 1 - \frac{\sigma(\delta_{max})}{\delta_{max}} \frac{1}{K_0} \tag{5}$$

PROPOSED METHODOLOGY

In this work, a new approach in the damage FE implementation of interfaces is proposed. First, it is not explicitly defined a damage law. Indeed, this relation is calculated at each step by using the experimental cohesive relationship, which is generated by interpolating some inputted points. These points are sampled from a traction-separation curve, obtained from previous (mode I or II) decohesion tests, and are inserted in an array named PARX. The damage D is evaluated at each step increment and is updated from the beginning of the loading process (when the decohesion displacement is yet null). The present tool allows to define damage variables that are independent for each fracture mode (i.e. anisotropic damage formulation).

For the sake of simplicity, we hereby describe only the analytical formulation of mode I cohesive law because the mode II cohesive relationship can be similarly defined. Thus, the components of the traction vector $\boldsymbol{T}$ of dominant mode I loading conditions are expressed by the following equations:

$$\sigma = \begin{cases} (1-D)K_{n0}\delta_n, \ \delta_n \geq 0 \\ K_{n0}\delta_n, \ \delta_n < 0 \end{cases} \tag{6}$$

$$\tau = (1-D)K_{s0}\delta_s \tag{7}$$

where D is the damage function and the initial stiffness K_{n0} and K_{s0} are the slope of the first segment of mode I and mode II cohesive curve, respectively.
The structure of the algorithm requires the displacement jump $\boldsymbol{u}$ and its relative increments $d\boldsymbol{u}$ as data input, whilst provides as output with σ, τ and its derivative respect to the displacement jump components.
For each integration step, the value of displacement jump across the interface δ_n is compared with the state variable δ_{max}, which is associated with the current damage (5), reported here:

$$\delta_{max} = \max_{\tau \in (0,t)} \{\delta(\tau)\}$$

where t is the variable time.
When separation is greater than previous δ_{max}, i.e. the point (δ_{curr}, σ_{curr}) is located on the effective limit curve $\sigma = f(\delta_n)$ (Fig. 4), the damage D is increasing according to the relationship

$$1 - D = \frac{K_{ncurr}}{K_{n0}} \tag{8}$$

Being δ_{curr} equal to the updated δ_{max}, the current stiffness is

$$K_{ncurr} = \frac{\sigma}{\delta_n} = \frac{f(\delta_{max})}{\delta_{max}} \tag{9}$$

whilst the initial stiffness

$$K_{n0} = f'(0) \tag{10}$$

Then, the stress field is recalculated according to Eqs. (6)-(7).

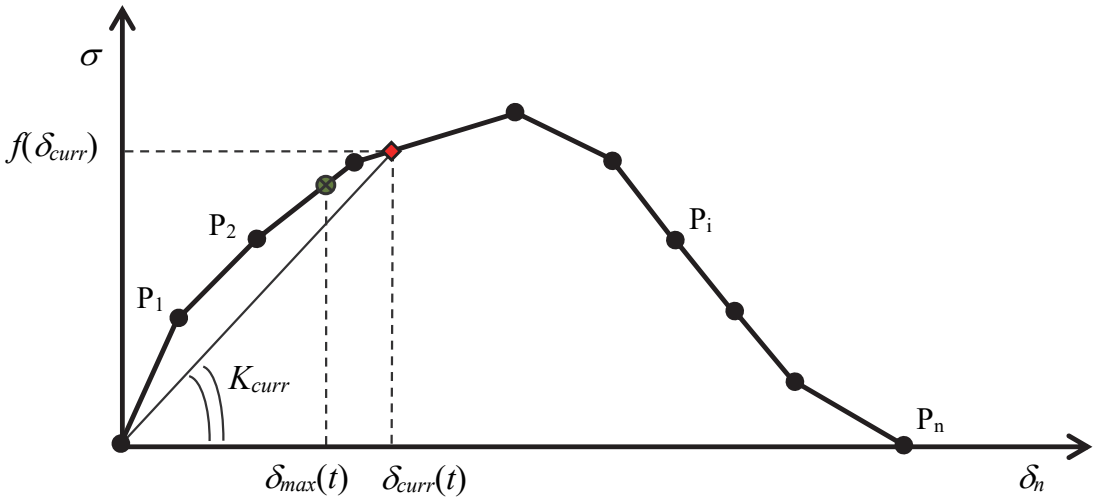

Figure 4: Interpolated cohesive law – opening of the interface.

The stress increment processed in FE iterations is equal to

$$\frac{d\sigma}{d\delta_n}=\begin{cases}(1-D)K_{n0}-K_{n0}\delta_n\dfrac{dD}{d\delta_n},\ \delta_n\geq 0\\ K_{n0},\ \delta_n<0\end{cases} \tag{11}$$

$$\frac{d\sigma}{d\delta_s}=0$$

$$\frac{d\tau}{d\delta_n}=0 \tag{12}$$

$$\frac{d\tau}{d\delta_s}=\begin{cases}(1-D)K_{s0}-K_{s0}\delta_s\dfrac{dD}{d\delta_s},\ \delta_s\geq 0\\ K_{s0},\ \delta_s<0\end{cases}$$

where

$$\frac{dD}{d\delta_n}=\begin{cases}-\dfrac{1}{f'(0)}\left(\dfrac{f'(\delta_n)\delta_n-f(\delta_n)}{\delta_n^2}\right),\ \delta_n=\delta_{max},d\delta_n\geq 0\\ 0,\ otherwise\end{cases} \tag{13}$$

$$\frac{dD}{d\delta_s}=0$$

A null derivative of damage with respect to separation δ_n implies that damage is considered constant and equal to the last estimated value when opening displacement at the interface is decreasing or $\delta_n < \delta_{max}$.
For this reason, if the current value of normal separation is less than previous δ_{max}, the corresponding point (δ_{curr}, σ_{curr}) is located inside the area under the effective limit curve and the damage D is considered unchanged (Fig. 5). The stress field is calculated using Eqs. (6)-(7).

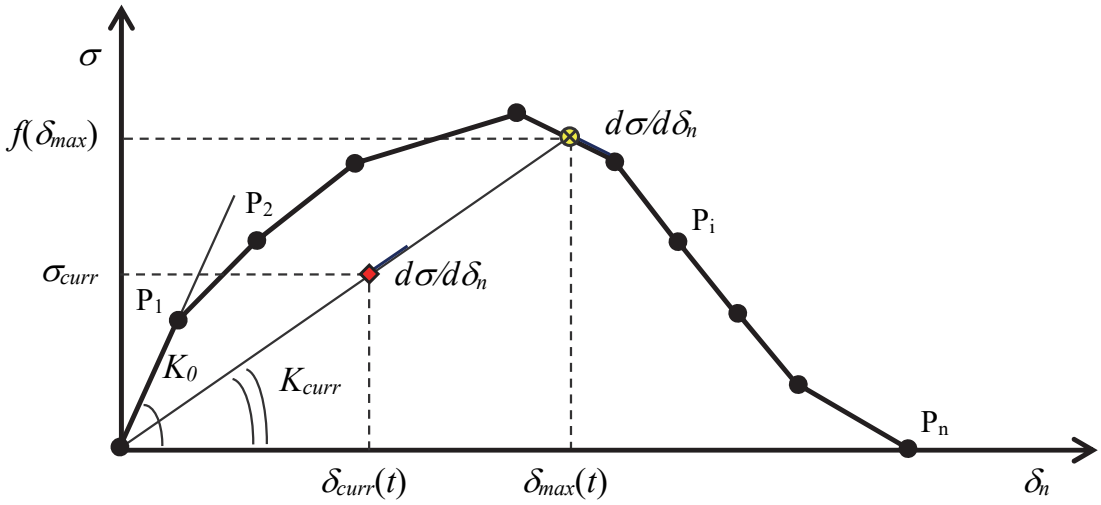

Figure 5: Interpolated cohesive law – closing of the interface.

A simplified flowchart of the proposed methodology in presented in Fig. 6.

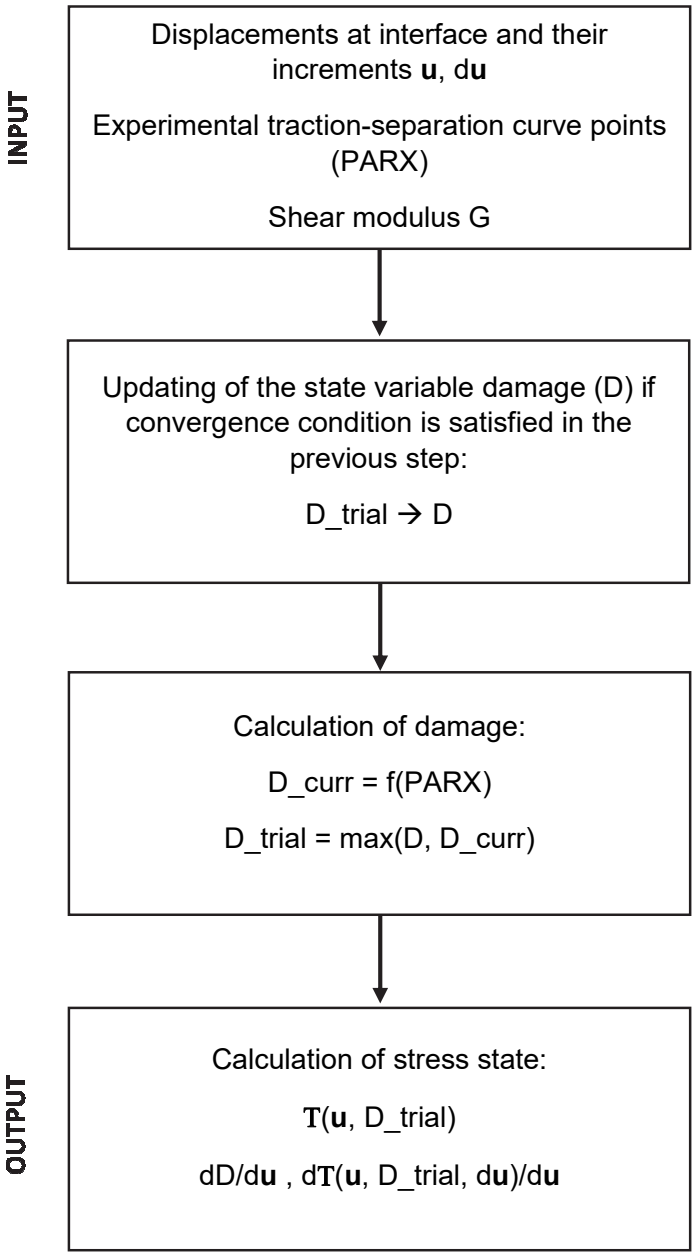

Figure 6: Overall schematic of algorithm, to be repeated until the convergence over **u** is achieved.

Although the stress field calculated using (6)-(7) is considered as obtained from a mode I fracture loading condition, i.e. the separation normal to the interface dominates the slip tangent to the interface, the developed algorithm can also evaluate the tangential stress (mode II) by means of a shear stiffness, function of *D*. Therefore, the stress field for a dominant mode II condition is obtained from the following equations:

$$\tau = \begin{cases} (1-D)K_{s0}\delta_s, & \delta_s \geq 0 \\ K_{s0}\delta_s, & \delta_s < 0 \end{cases} \tag{14}$$

$$\sigma = (1-D)K_{n0}\delta_n \tag{15}$$

where

$$1-D=\frac{K_{scurr}}{K_{s0}}. \tag{16}$$

The tangential slip distance is a numerical input from each FE iteration. When the dominant mode II loading condition is analysed, an experimental cohesive law shear τ - separation δ_s is to be used whilst the methodology follows the same scheme.

CASE STUDY

The proposed CZ model is implemented into the Abaqus FEM code through the user subroutine UINTER. A validation of the algorithm is presented simulating a case study, whose 2D geometry consists of a T-beam bonded to a clamped edge plate. The adopted case study is representative of all the main aspects and critical issues involved in debonding phenomenon of adhesive layer. Four different boundary conditions on displacements (see Fig. 7) are sequentially imposed to the web edge of the T-beam:

1) Opposing displacements to apply a clockwise moment;
2) Opposing displacements to apply an anticlockwise moment;
3) Null displacement (unloading step);
4) Tensile displacement.

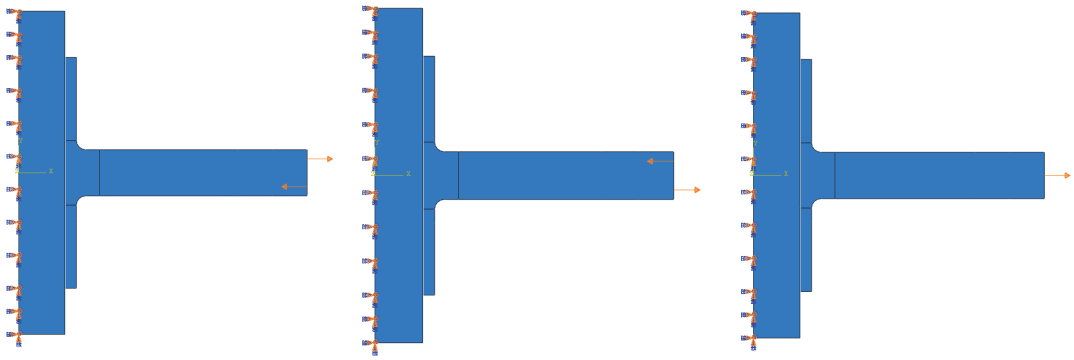

Figure 7: Boundary conditions on web edge displacements: step 1, step 2 and step 4, respectively.

The beam and the plate are considered made of steel, whilst the simulated adhesive is corresponding to the epoxy resin Araldite® 2015. Their elastic properties are listed in Tab. 1.

Material	E [GPa]	ν
Steel	210	0.30
Araldite® 2015	1.85	0.33

Table 1: Adherend and adhesive mechanical properties.

The bonded joint is modelled with about 3000 CPS4 elements (Fig. 8). The adhesive interface is modelled using cohesive elements with zero thickness; the considered CZM initial stiffness values are listed in Tab. 2.

K_{nn}	K_{ss}	K_{tt}
6476	2496	0

Table 2: CZM initial stiffness values set in FE simulations.

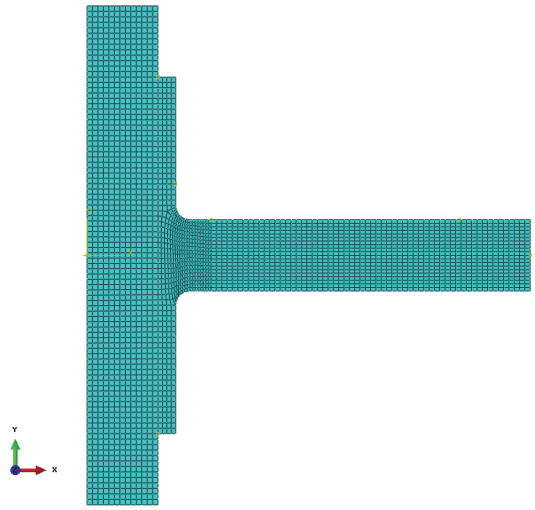

Figure 8: FE model mesh.

The experimental points used for the built up of the piecewise linear cohesive law, as explained in the methodology paragraph, are taken from the mode I decohesion test outcomes in [21].

RESULTS AND DISCUSSION

The plots of deformed bonded joint at different steps are shown in Fig. 9. The debonding phenomenon occurs since the application of first loading condition. The relationship between traction and separation of representative points at the interface is depicted in Fig. 10. It is possible to highlight a cohesive behaviour, which includes the phases of damage propagation complete debonding, and constant damage.

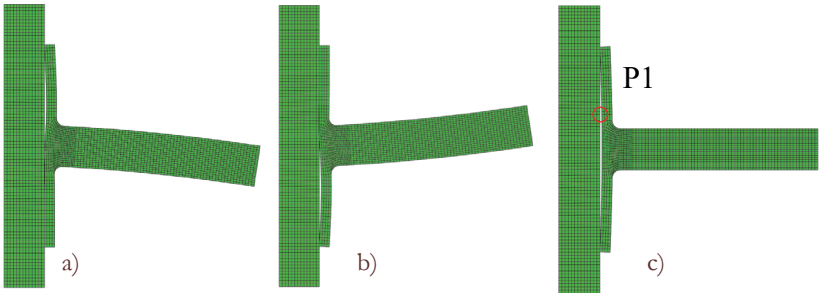

Figure 9: Deformed mesh plots at step 1, step 2 and step 4, respectively.

In particular, in the representative point P1, a complete debonding is reaching during step 1 (Fig. 9-a), when a clockwise moment is applied, strictly following the cohesive behaviour as expressed by the experimental law. The normal separation, after the debonding, reaches the value of about 0.06 mm maintaining the stress equal to zero. Subsequently, when an anticlockwise moment is applied to the specimen, the trend of normal displacement highlights the interface closure of the upper part of flange (Fig. 9-b) and the cohesive stress increases in compression, following the slope of K_{n0}, up to the value of about 19 MPa. During the step 3, there is the unloading phase of the entire specimen and stress and separation return to zero. Finally, when a tensile displacement is applied to the bonded joint for highlighting the interface opening (Fig. 9-c), the corresponding cohesive traction remains equal to zero nevertheless the separation increases up to the value of about 0.045 mm. Moreover, the hypothesis of case study under dominant mode I load condition is confirmed comparing the components of the traction vector. Indeed, as verifiable in Fig. 10, the value of tangential traction is negligible during the entire load spectrum with respect to the traction normal to the interface.

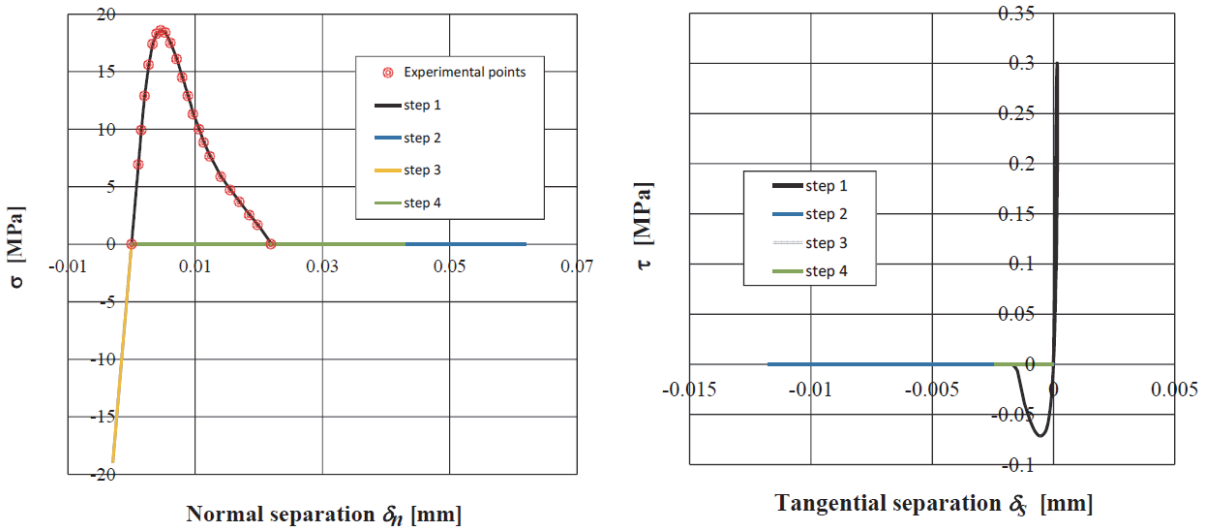

Figure 10: Traction-separation curves (σ–δ_n and τ–δ_s) of the representative point P1 at the interface.

The damage evolution is evaluated from the beginning of the loading process, trying to better simulate the real process of decohesion. Although the tabular definition of damage as function of displacement is available in Abaqus, there is no possibility to use uncoupled damage functions, which refer to different fracture modes. With the proposed tool, instead, it is possible to define a specific damage function for each fracture mode.
Finally, good convergence properties of the algorithm have been shown during FEM simulations, allowing the authors to consider the described methodology to be efficient and robust.

Conclusions

The cohesive zone modelling of an adhesively bonded joint is analyzed by using an innovative straightforward methodology implemented into a commercial finite element code. Experimental results from standard fracture tests, in terms of traction-separation law, are used as an input for the algorithm but no damage law has to be explicitly defined. In such a way, the in-house developed algorithm calculates the damage at each step increment, from the beginning of loading process, when decohesion opening displacement is yet null, up to the complete debonding of the joint. A case study for validation is presented by using the software Abaqus. The cohesive behaviour in the interface elements of bonded joint is shown over all different loading conditions (damage propagation, constant damage and complete debonding), providing with satisfactory results.

References

[1] Ascione L., Berardi V.P., Anchorage device for FRP laminates in the strengthening of concrete structures close to beam-column joints, Composites Part B: Engineering, 42(7) (2011) 1840-1850.
[2] Corato V., Affinito L., Anemona A., Besi Vetrella U., della Corte A., Di Zenobio A., Fiamozzi Zignani C., Freda R., Messina G., Muzzi L., Perrella M., Reccia L., Tomassetti G., Turtù S., Detailed design of the large-bore 8T superconducting magnet for the NAFASSY test facility, Superconductor Science and Technology, 28(3) (2015) 034005. DOI:10.1088/0953-2048/28/3/034005.
[3] Campilho R.D.S.G., de Moura M.F.S.F., Domingues J.J.M.S., Using a cohesive damage model to predict the tensile behaviour of CFRP single-strap repairs, International Journal of Solids and Structures, 45 (2008) 1497-1512.
[4] Cricrì, G., Luciano, R., Homogenised properties of composite materials in large deformations, Composite Structures, 103 (2013) 9-17.
[5] Cricrì, G., A consistent use of the Gurson-Tvergaard-Needleman damage model for the R-curve calculation, Frattura ed Integrità Strutturale, 24 (2013) 161-174.
[6] Calì, C., Cricrì, G., Perrella, M., An advanced creep model allowing for hardening and damage effects, Strain, 46(4) (2010) 347-357.

[7] Valoroso N., de Barros S., Adhesive joint computations using cohesive zones, Applied Adhesion Science, 1 (2013) 1-9. DOI:10.1186/2196-4351-1-8.
[8] Citarella, R., Cricrì, G., Three-dimensional BEM and FEM submodelling in a cracked FML full scale aeronautic panel, Applied Composite Materials, 21(3) (2014) 557-577.
[9] Olsson P., Stigh U., On the determination of the constitutive properties of thin interphase layers - an exact inverse solution, International Journal of Fracture, 41 (1989) 71-76.
[10] Sørensen B.F., Jacobsen T.K., Determination of cohesive laws by the J integral approach, Engineering Fracture Mechanics, 70 (2003) 1841-1858.
[11] Valoroso N., Sessa S., Lepore M., Cricrì G., Identification of mode-I cohesive parameters for bonded interfaces based on DCB test, Engineering Fracture Mechanics, 104 (2013) 56-79.
[12] Stigh U., Andersson T., An experimental method to determine the stress-elongation relation for a structural adhesive loaded in peel, European Structural Integrity Society, 27 C (2000) 297-306.
[13] Shen B., Paulino G.H., Direct Extraction of Cohesive Fracture Properties From Digital Image Correlation: A Hybrid Inverse Technique, Experimental Mechanics, 51 (2011) 143-163.
[14] Fernandes R.M.R.P., Chousal J.A.G., de Moura M.F.S.F., Xavier J., Determination of cohesive laws of composite bonded joints under mode II loading, Composites: Part B, 52 (2013) 269-274.
[15] Leffler, K., Alfredsson, K.S., Stigh, U., Shear behaviour of adhesive layers, International Journal of Solids and Structures, 44(2) (2007) 530-545.
[16] Högberg, J.L., Sørensen, B.F., Stigh, U., Constitutive behaviour of mixed mode loaded adhesive layer, International Journal of Solids and Structures, 44(25-26) (2007) 8335-8354.
[17] Khoshravan, M.R., Moslemi, M., Investigation on mode III interlaminar fracture of glass/epoxy laminates using a modified split cantilever beam test, Engineering Fracture Mechanics, 127 (2014) 267-279.
[18] Cricrì G., Perrella M., Sessa S., Valoroso N., A novel fixture for measuring mode III toughness of bonded assemblies, Engineering Fracture Mechanics, 138 (2015), 1-18. DOI: 10.1016/j.engfracmech.2015.03.019.
[19] Tvergaard V., Hutchinson J.W., The relation between crack growth resistance and fracture process parameters in elastic-plastic solids, Journal of the Mechanics and Physics of Solids, 40 (1992) 1377-1397.
[20] Needleman, A., An analysis of decohesion along an imperfect interface, International Journal of Fracture, 42 (1990) 21-40.
[21] de Moura M.F.S.F., Gonçalves J.P.M., Magalhães A.G., A straightforward method to obtain the cohesive laws of bonded joints under mode I loading, International Journal of Adhesion and Adhesives, 39 (2012) 54-59.